## **OPEN ACCESS**



# A Significant Detection of X-ray Polarization in Sco X-1 with PolarLight and Constraints on the Corona Geometry

Xiangyun Long<sup>1</sup>, Hua Feng<sup>2,1</sup>, Hong Li<sup>2</sup>, Jiahuan Zhu<sup>2</sup>, Qiong Wu<sup>1</sup>, Jiahui Huang<sup>1</sup>, Massimo Minuti<sup>3</sup>, Weichun Jiang<sup>4</sup>, Dongxin Yang<sup>1</sup>, Saverio Citraro<sup>3</sup>, Hikmat Nasimi<sup>3</sup>, Jiandong Yu<sup>5</sup>, Ge Jin<sup>6</sup>, Ming Zeng<sup>1</sup>, Peng An<sup>5</sup>, Jiachen Jiang<sup>2</sup>, Enrico Costa<sup>7</sup>, Luca Baldini<sup>3</sup>, Ronaldo Bellazzini<sup>3</sup>, Alessandro Brez<sup>3</sup>, Luca Latronico<sup>8</sup>, Carmelo Sgrò<sup>3</sup>, Gloria Spandre<sup>3</sup>, Michele Pinchera<sup>3</sup>, Fabio Muleri<sup>7</sup>, and Paolo Soffitta<sup>7</sup>, Department of Engineering Physics, Tsinghua University, Beijing 100084, People's Republic of China Department of Astronomy, Tsinghua University, Beijing 100084, People's Republic of China; hfeng@tsinghua.edu.cn

<sup>3</sup> INFN-Pisa, Largo B. Pontecorvo 3, I-56127 Pisa, Italy

<sup>4</sup> Key Laboratory for Particle Astrophysics, Institute of High Energy Physics, Chinese Academy of Sciences, Beijing 100049, People's Republic of China

<sup>5</sup> School of Electronic and Information Engineering, Ningbo University of Technology, Ningbo, Zhejiang 315211, People's Republic of China

<sup>6</sup> North Night Vision Technology Co., Ltd., Nanjing 211106, People's Republic of China

<sup>7</sup> IAPS/INAF, Via Fosso del Cavaliere 100, I-00133 Rome, Italy

<sup>8</sup> INFN, Sezione di Torino, Via Pietro Giuria 1, I-10125 Torino, Italy

<sup>8</sup> INFN, Sezione di Torino, Via Pietro Giuria 1, I-10125 Torino, Italy

<sup>8</sup> INFN, Sezione di Torino, Via Pietro Giuria 1, I-10125 Torino, Italy

## **Abstract**

We report the detection of X-ray polarization in the neutron-star low-mass X-ray binary Scorpius (Sco) X-1 with PolarLight. The result is energy-dependent, with a nondetection in 3–4 keV but a  $4\sigma$  detection in 4–8 keV; it is also flux-dependent in the 4–8 keV band, with a nondetection when the source displays low fluxes but a  $5\sigma$  detection during high fluxes, in which case we obtain a polarization fraction of  $0.043 \pm 0.008$  and a polarization angle of  $52^{\circ}.4$ . This confirms a previous marginal detection with OSO-8 in the 1970s and marks Sco X-1 as the second astrophysical source with a significant polarization measurement in the keV band. The measured polarization angle is in line with the jet orientation of the source on the sky plane ( $54^{\circ}$ ), which is supposedly the symmetry axis of the system. Combining previous spectral analysis, our measurements suggest that an optically thin corona is located in the transition layer under the highest accretion rates, and disfavor the extended accretion disk corona model.

*Unified Astronomy Thesaurus concepts:* Polarimetry (1278); Low-mass x-ray binary stars (939); Neutron stars (1108); Accretion (14)

### 1. Introduction

Sco X-1 is the first discovered extrasolar X-ray source (Giacconi et al. 1962) and the brightest persistent object in the keV sky besides the Sun. It is a low-mass X-ray binary (LMXB) containing a neutron star (Steeghs & Casares 2002) with an orbital period of 0.787 days (Galloway et al. 2014) at a distance of 2.13 kpc (Arnason et al. 2021). The source is classified as a so-called Z source based on its evolutionary pattern on the color-color diagram (Hasinger & van der Klis 1989). Sco X-1 represents a class of LMXBs with high accretion rates, with a peak luminosity of around  $2 \times 10^{38}$ erg s<sup>-1</sup>, which is close to the Eddington limit of a  $1.4 M_{\odot}$ neutron star (Titarchuk et al. 2014). Unlike black holes, the hard surface of neutron stars will stop the accretion flow and dissipate the energy that can otherwise be swallowed by the event horizon. Therefore, a transition layer, or similarly a spreading layer or a boundary layer, is expected in between the Keplerian accretion disk and the star surface (Inogamov & Sunyaev 1999). The existence of such a layer is supported by X-ray timing (Sunyaev & Revnivtsev 2000).

X-ray studies of Sco X-1 have been conducted mainly with the Rossi X-ray Timing Explorer (RXTE) in the energy range from about 3 keV to a few hundred keV because the extreme

Original content from this work may be used under the terms of the Creative Commons Attribution 4.0 licence. Any further distribution of this work must maintain attribution to the author(s) and the title of the work, journal citation and DOI.

brightness of the source may saturate most of the detectors behind focusing telescopes. The energy spectrum of Sco X-1 can be decomposed into several components: a thermal component possibly from the inner accretion disk or the neutron-star surface, an iron emission line, and a dominant Comptonization component (Barnard et al. 2003; Bradshaw et al. 2003; D'Aí et al. 2007; Church et al. 2012; Titarchuk et al. 2014). Based on X-ray dipping and other evidence for the corona size, an extended accretion disk corona model is proposed for X-ray Comptonization in LMXBs (Church & Bałucińska-Church 2004) as well as in Sco X-1 (Barnard et al. 2003; Church et al. 2012). However, spectral analysis reveals that the seed photons for Comptonization may have a temperature exceeding the maximum temperature of the accretion disk. Thus, the seed photons likely originate from the neutron-star surface, and consequently, the corona is located in the transition layer (D'Aí et al. 2007; Titarchuk et al. 2014). This scenario is favored by studies with frequencyresolved spectroscopy (Revnivtsev & Gilfanov 2006). It is also suggested that a corona in the transition layer can up-scatter seed photons from both the disk and neutron-star surface (Titarchuk et al. 2014).

X-ray polarimetry is sensitive to the geometry in radiation transfer and may help distinguish different corona models (Schnittman & Krolik 2010). The Bragg polarimeter on OSO-8 observed Sco X-1 in the 1970s (Long et al. 1979) and produced a nondetection around 2.6 keV but a  $3\sigma$  measurement around 5.2 keV with a polarization fraction (PF) of  $0.0131 \pm 0.0040$ 

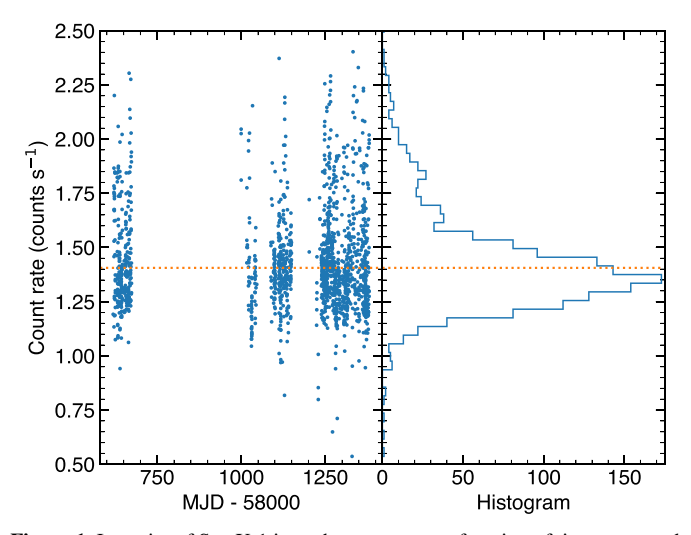


**Figure 1.** Intensity of Sco X-1 in each exposure as a function of time measured with PolarLight in the energy range of 2–8 keV and a histogram of the intensity. The dashed line marks the level to separate the low- and high-intensity exposures, with approximately the same number of counts in each segment.

and a polarization angle (PA) of  $57^{\circ} \pm 6^{\circ}$ . Launched in 2018, PolarLight is the second dedicated astrophysical X-ray polarimeter in the keV band (Feng et al. 2019). We thereby conducted polarization measurements of Sco X-1 with PolarLight after we finished observations of the Crab Nebula (Feng et al. 2020; Long et al. 2021). In this paper, we report a significant detection of polarization and discuss how the result can help constrain the location and geometry of the corona in Sco X-1.

## 2. Observations and Analysis

Sco X-1 has been observed with PolarLight in four time epochs, from 2019 May 14 to 2019 July 09, 2020 May 30 to 2020 July 16, 2020 August 27 to 2020 October 29, and 2021 January 10 to 2021 June 15, with a total exposure of 884 ks. The first two observing windows were scheduled during the Sun avoidance for observations of the Crab Nebula. In 2020 August, the monitoring program for the Crab Nebula ended and Sco X-1 became the primary target of PolarLight. In late 2020, the schedule was interrupted in response to a target of opportunity. After 2021 mid-June, the instrument turned to

observe another target of opportunity. A continuous exposure with PolarLight typically lasts 10 minutes. The exposure-by-exposure lightcurve is shown in Figure 1 with a histogram of the source intensity (count rate).

The data reduction is the same as that employed in the analysis for the Crab observations (Long et al. 2021). A valid event contains an image of energy deposit, i.e., the track image. The background events are screened using an energy-dependent algorithm (Zhu et al. 2021). Some background events are produced by secondary electrons with an energy close to the X-rays of interest and are thus not removable. Events with at least 58 pixels and located in the central  $\pm 7$  mm region of the detector are selected for analysis.

The energy of X-rays, or precisely, the relation between the energy and analog-to-digital numbers, may vary with time and is calibrated by comparing the measured and simulated source spectra (Li et al. 2021). For this purpose, one needs to assume an incident source spectrum. However, Sco X-1 displays spectral variability that may affect the accuracy of the calibration. Titarchuk et al. (2014) performed a comprehensive spectral study of the source with RXTE observations at different spectral branches. Fortunately, the variation in spectral shape in our energy band is not dramatic. We plot all these spectral models and find the "typical" one that has a median spectral slope in 2–8 keV. This one catches the source in the normal branch. Then, we take the 5th and 95th percentile spectra ordered by the spectral slope as two extremes. The X-ray energies calibrated against the typical spectrum and the two extremes differ by a factor less than 10% in 2–8 keV. This is less than the energy resolution (23% around 2 keV and 16%) around 8 keV, full width at half maximum) of the detector and can be ignored.

The emission angle of photoelectrons is inferred using the impact-point method (Bellazzini et al. 2003). The average modulation factors in different energy bands (see Table 1) are calculated based on the laboratory calibrations (Feng et al. 2019) weighted by the measured source spectrum. The background fraction during on-source observations is estimated to be on the order of 1%, also listed in Table 1. Identical to previous studies (Feng et al. 2020; Long et al. 2021), we calculate the polarization based on the Stokes parameters (Kislat et al. 2015; Mikhalev 2018), and infer the intrinsic PF and PA using a Bayesian approach (Maier et al. 2014; Mikhalev 2018) that is immune from the bias in polarization

 Table 1

 X-ray Polarization Measurements of Sco X-1 with PolarLight

Energy (keV)	Intensity	$N_{ m ph}$	$f_{b}$	MDP	PF	PA (°)
(1)	(2)	(3)	(4)	(5)	(6)	(7)
3–4	all	353558	0.007	0.022	$0.000^{+0.011}_{-0.000}$	$40.0 \pm 29.3$
4–8	all	282822	0.017	0.018	$0.026^{+0.006}_{-0.006}$	$56.4 \pm 6.7$
3–4	low	176211	0.008	0.031	$0.008^{+0.009}_{-0.008}$	$5.2 \pm 26.6$
4–8	low	134579	0.019	0.026	$0.000^{+0.011}_{-0.000}$	$77.8 \pm 36.1$
3–4	high	177347	0.006	0.031	$0.018^{+0.010}_{-0.012}$	$62.2 \pm 18.1$
4–8	high	148243	0.015	0.025	$0.043^{+0.008}_{-0.008}$	$52.6 \pm 5.4$

Note. Column (1): energy range. Column (2): intensity range. Column (3): total number of events used for polarization analysis. Column (4): fraction of background events estimated in this energy and intensity interval. Column (5): the minimum detectable polarization (MDP) at 99% confidence level, =  $4.29/[\mu(1-f_b)\sqrt{N_{ph}}]$ , where  $\mu$  is the modulation factor or the fractional modulation amplitude in response to fully polarized X-rays, about 0.33 in 3–4 keV and 0.46 in 4–8 keV. Column (6): polarization fraction. Column (7): polarization angle in degree. Errors are quoted as 68% credible intervals.

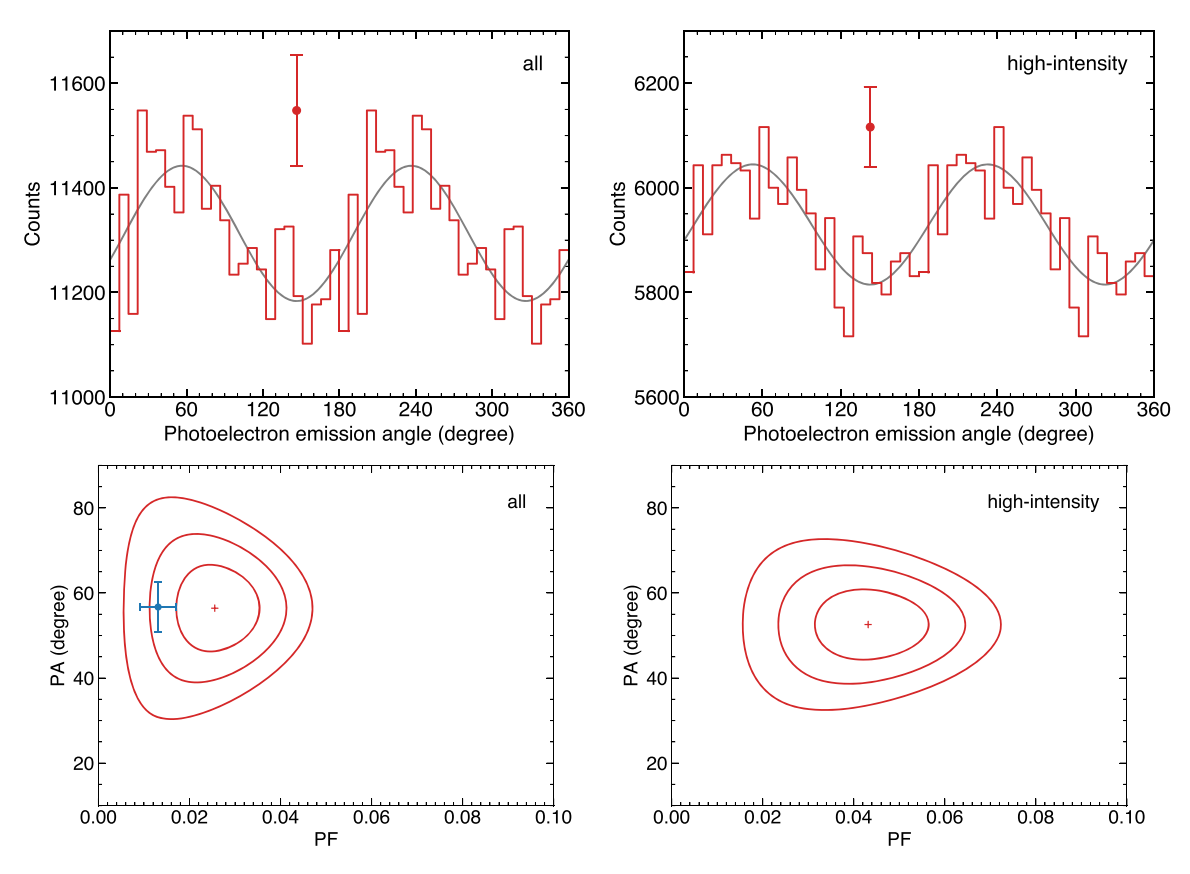
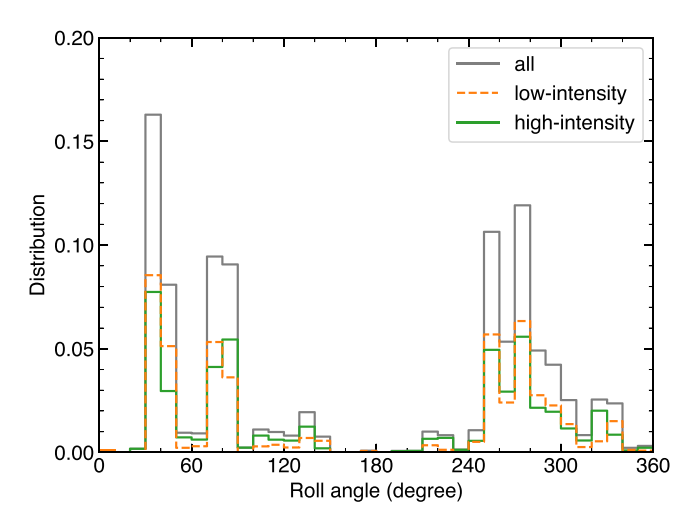


Figure 2. Polarimetric modulation curves (red histograms) and corresponding PA versus PF contours of Sco X-1 in the 4–8 keV band, in all and the high-intensity time intervals, respectively. Top: the modulation curves are for visual inspection only, with typical  $1\sigma$  error bars, and the model curves (gray lines) are derived from the Stokes/Bayesian analysis. Bottom: the red crosses indicate the point estimates and the contours encircle the  $1\sigma$ ,  $2\sigma$ , and  $3\sigma$  credible intervals of the Bayesian posterior distribution. The blue point with error bars marks the measurement obtained with OSO-8 around 5.2 keV.

analysis. The marginalized posterior distribution is used for parameter estimates. The credible interval is calculated as the region with the highest posterior density.

The polarization measurement is performed in two energy bands, 3–4 and 4-8 keV, respectively. The analysis in 3–4 keV yields a PF consistent with zero, while the PF measured in 4–8 keV has a significance of  $4\sigma$ . Due to the small effective area and relatively narrow band of PolarLight, it is not possible to calculate the color-color or hardness-intensity diagram for branch identification on the timescales suited for that purpose. The data therefore cannot be categorized based on position on the Z-track. Instead, we opt to divide the data into two segments (low/high intensity) based solely on the intensity in the exposure in a way that produces approximately the same number of counts in both segments. This ensures that the two segments have almost the same sensitivity in polarization measurement. As Sco X-1 exhibits similar intensities in the horizontal and normal branches, but a higher intensity in the flaring branch (Titarchuk et al. 2014), the two data sets can still be expected to correlate with the position in the Z-track.

In the 4–8 keV energy range, the low-intensity half shows a PF consistent with zero, while a  $5\sigma$  detection is obtained with the high-intensity data, with PF =  $0.043 \pm 0.008$  and PA =  $52^{\circ}.6 \pm 5^{\circ}.4$ . The significance that we quote is purely statistical, and is verified to be consistent with the sensitivity (MDP) of the observation given the number of photons and modulation factor (Weisskopf et al. 2010; Strohmayer & Kallman 2013). The polarization measurements in different energy bands and intensity intervals are listed in Table 1. The



**Figure 3.** Distribution of the PolarLight roll angle during observations of Sco X-1 and those when the source displays low and high intensities.

modulation curves and PA versus PF contours are shown in Figure 2. Our measurement in the 4–8 keV band in all intensity intervals is consistent with that obtained with OSO-8 around 5.2 keV.

# 2.1. Arguments against Background or Systematic Effects

We present evidence that the polarization measurements are not affected by the background or instrument systematics. The background count rate is too low for us to constrain any

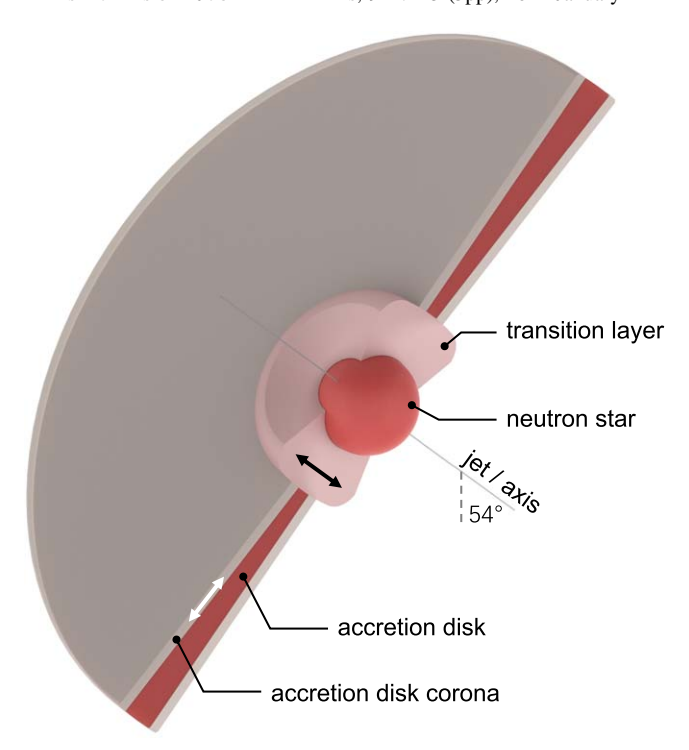


**Figure 4.** Schematic drawing of the accretion flow and expected polarization angles of the two models. The radio jet has an orientation of  $54^{\circ}$  on the sky plane and is likely the symmetry axis of the accretion flow. Given an optically thin corona, if the Comptonization occurs in the accretion disk corona, the PA is expected to be aligned with the disk plane, as indicated by the white arrow; otherwise, if the Comptonization occurs in the transition layer, the PA is expected to be in line with the system axis, as indicated by the black arrow.

spurious modulation in it. The background fraction is estimated to be about 1.5% in 4–8 keV during high-intensity intervals. Even if it is 100% polarized, it cannot produce a PF as high as 0.043 as observed. Furthermore, if the detection is due to background effects, it should be more significant at low-intensity intervals rather than in high-intensity intervals. To conclude, a significant background effect on the detection can be ruled out.

Unpolarized X-rays may result in a residual modulation in a pattern similar to that caused by polarization. Such an instrument systematics at 5.9 keV is lower than 1% averaged over the detector plane for this type of detector (Li et al. 2015). For PolarLight, the response to an unpolarized beam, 5.9 keV from an <sup>55</sup>Fe source, has been found to be low, with a 90% upper limit of 0.016 on PF. Any instrument rotation, such as from the roll pattern shown in Figure 3, would further suppress such a residual modulation. We find that by folding with the roll pattern in either the low- or high-intensity intervals, the amplitude of modulation is lowered by a factor of 2. Considering that the low- and high-intensity data sets have the same energy range, comparable sensitivity for polarization measurements, and similar roll-angle distributions, it is unlikely for a systematic effect from the unpolarized response to appear significantly in one data set but not in the other. Also, the instrument systematics, if any, are only significant in the energy band below 4 keV (Baldini et al. 2021); a nondetection in the low-energy band but a significant detection in the high-energy band does not reconcile with the behavior of such an effect.

Furthermore, the independent measurements with PolarLight and OSO-8 produce a consistent PA within errors,  $52^{\circ}.6 \pm 5^{\circ}.4$  versus  $57^{\circ} \pm 6^{\circ}$ . This further strengthens the reliability of the

results, as the PA measurement is a pure geometric effect, almost not affected by calibration uncertainties.

#### 3. Discussion

The measured PA is in line with the orientation (54° from north to east) of the radio jet on the sky plane (Fomalont et al. 2001). It is reasonable to assume that the jet is perpendicular to the inner accretion disk. Therefore, the PA is perpendicular to the disk, i.e., parallel with the symmetry axis of the system. In the energy range of a few keV, the flux fraction from the Comptonization component increases with energy (D'Aí et al. 2007). A nondetection at low energies and a significant detection toward high energies suggests that the thermal emission is intrinsically of low polarization and the signal is a result of scattering in the corona. Spectral modeling uncovers that the corona of Sco X-1 is optically thin at the highest luminosities (D'Aí et al. 2007), with an optical depth below 1 in some of the flaring branch and as low as 0.1 on the top of the flaring branch. In this case, the average number of scatters is less than unity, and the PA can be inferred from the geometry as follows. If the corona is flat and extended above the disk, with seed photons from the disk beneath, a PA perpendicular to the system axis is expected. Otherwise, if the corona resides in the transition layer, then the PA is expected to be parallel with the system axis or the radio jet. A physical picture of the accretion system is illustrated in Figure 4.

The signature of X-ray polarization with a wedge-like corona above the accretion disk (sandwich geometry) around a stellarmass black hole has been studied with simulation (Schnittman & Krolik 2010). This is similar to the geometry of the accretion disk corona discussed above and may be used for an informative comparison despite a neutron star in Sco X-1. The polarization is found to be parallel with the disk plane if the photons are scattered once, but perpendicular to it with multiple scatters (Schnittman & Krolik 2010). Considering the low optical depth and a seed photon temperature of 2-3 keV (corresponding to a thermal peak at 5–8 keV; D'Aí et al. 2007), the majority of the scattered photons in 4-8 keV should be scattered only once in the corona (Rybicki & Lightman 1986), leading to the same conclusion as discussed above. Simulations assuming an active galactic nucleus (Beheshtipour et al. 2017) may not be applicable to our case because the seed photon temperature is much lower. If there are multiple scatters, although the PA fits the measurement, their simulations indicate that the PF decreases with increasing luminosity (Schnittman & Krolik 2010), opposite to what we have found.

A spherical corona with seed photons from a truncated disk is also investigated (Schnittman & Krolik 2010). This is slightly different from the geometry of a transition-layer corona, where the spherical caps are removed and the thermal emission from the neutron-star surface could be another important seed (see Figure 4). A sphere without caps breaks the symmetry and can help increase the observed PF. The average PA after scattering in a spherical corona is expected to be perpendicular to the disk, and the perpendicular component mainly originates from the portion of corona at low latitudes and relatively large radii, i.e., in the region occupied by the transition-layer corona (see Figure 12 in Schnittman & Krolik 2010). Therefore, the simulation results agree with our first principle analysis. To conclude, the polarization measurements favor the scenario where an optically thin corona is

located in the transition layer when the source undergoes high accretion rates.

Nevertheless, to better understand the physics and geometry, dedicated simulations are needed. This work implies that, especially for the study of systems with low strength of magnetic fields, it is important to have time- and energy-resolved X-ray polarimetry, as well as broadband spectroscopy to determine the emission state to break the degeneracy in the model. These can be fulfilled with future missions (Weisskopf et al. 2016; Zhang et al. 2019).

We thank the anonymous referees for useful comments. H.F. acknowledges funding support from the National Natural Science Foundation of China (grants Nos. 11633003, 12025301, and 11821303), the CAS Strategic Priority Program on Space Science (grant No. XDA15020501-02), the National Key R&D Project (grants No. 2018YFA0404502), and the Tsinghua University Initiative Scientific Research Program.

## **ORCID iDs**

Hua Feng https://orcid.org/0000-0001-7584-6236
Luca Baldini https://orcid.org/0000-0002-9785-7726
Ronaldo Bellazzini https://orcid.org/0000-0002-2469-7063
Luca Latronico https://orcid.org/0000-0002-0984-1856
Carmelo Sgrò https://orcid.org/0000-0001-5676-6214
Fabio Muleri https://orcid.org/0000-0003-3331-3794
Paolo Soffitta https://orcid.org/0000-0002-7781-4104

### References

Arnason, R. M., Papei, H., Barmby, P., Bahramian, A., & Gorski, M. D. 2021, MNRAS, 502, 5455

```
Baldini, L., Barbanera, M., Bellazzini, R., et al. 2021, APh, 133, 102628
Barnard, R., Church, M. J., & Bałucińska-Church, M. 2003, A&A, 405, 237
Beheshtipour, B., Krawczynski, H., & Malzac, J. 2017, ApJ, 850, 14
Bellazzini, R., Angelini, F., Baldini, L., et al. 2003, Proc. SPIE, 4843, 383
Bradshaw, C. F., Geldzahler, B. J., & Fomalont, E. B. 2003, ApJ, 592, 486
Church, M. J., & Bałucińska-Church, M. 2004, MNRAS, 348, 955
Church, M. J., Gibiec, A., Bałucińska-Church, M., & Jackson, N. K. 2012,
        . 546, A35
D'Aí, A., Życki, P., Di Salvo, T., et al. 2007, ApJ, 667, 411
Feng, H., Jiang, W., Minuti, M., et al. 2019, ExA, 47, 225
Feng, H., Li, H., Long, X., et al. 2020, NatAs, 4, 511
Fomalont, E. B., Geldzahler, B. J., & Bradshaw, C. F. 2001, ApJ, 558, 283
Galloway, D. K., Premachandra, S., Steeghs, D., et al. 2014, ApJ, 781, 14
Giacconi, R., Gursky, H., Paolini, F. R., & Rossi, B. B. 1962, PhRvL, 9, 439
Hasinger, G., & van der Klis, M. 1989, A&A, 225, 79
Inogamov, N. A., & Sunyaev, R. A. 1999, AstL, 25, 269
Kislat, F., Clark, B., Beilicke, M., & Krawczynski, H. 2015, APh, 68, 45
Li, H., Feng, H., Muleri, F., et al. 2015, NIMPA, 804, 155
Li, H., Long, X., Feng, H., et al. 2021, AdSpR, 67, 708
Long, K. S., Chanan, G. A., Ku, W. H. M., & Novick, R. 1979, ApJL,
   232, L107
Long, X., Feng, H., Li, H., et al. 2021, ApJL, 912, L28
Maier, D., Tenzer, C., & Santangelo, A. 2014, PASP, 126, 459
Mikhalev, V. 2018, A&A, 615, A54
Revnivtsev, M. G., & Gilfanov, M. R. 2006, A&A, 453, 253
Rybicki, G. B., & Lightman, A. P. 1986, Radiative Processes in Astrophysics
   (New York, NY: Wiley)
Schnittman, J. D., & Krolik, J. H. 2010, ApJ, 712, 908
Steeghs, D., & Casares, J. 2002, ApJ, 568, 273
Strohmayer, T. E., & Kallman, T. R. 2013, ApJ, 773, 103
Sunyaev, R., & Revnivtsev, M. 2000, A&A, 358, 617
Titarchuk, L., Seifina, E., & Shrader, C. 2014, ApJ, 789, 98
Weisskopf, M. C., Elsner, R. F., & O'Dell, S. L. 2010, Proc. SPIE, 7732,
Weisskopf, M. C., Ramsey, B., O'Dell, S., et al. 2016, Proc. SPIE, 9905,
   990517
Zhang, S., Santangelo, A., Feroci, M., et al. 2019, SCPMA, 62, 29502
Zhu, J., Li, H., Feng, H., et al. 2021, RAA, 21, 233
```